LG₁₁-mode vortex Nd:YAG laser by applying second-order circular Dammann grating for annular pumping

Quan Zhang (张 权)[1,2], Junjie Yu (余俊杰)[1], Biran Shi (施必然)[1,2], Fanchun Tang (唐凡春)[1,2], and Jianlang Li (李建郎)[1,*]

[1]*Shanghai Institute of Optics and Fine Mechanics, Chinese Academy of Sciences, Shanghai 201800, China*
[2]*Center of Materials Science and Optoelectronics Engineering, University of Chinese Academy of Sciences, Beijing 100049, China*
Corresponding author: apuli@siom.ac.cn

The excitation of high-order Laguerre–Gaussian (LG) modes in a neodymium-doped yttrium aluminum garnet (Nd:YAG) laser resonator was presented by applying the diffraction of a second-order circular Dammann grating (CDG) for annular pumping. In the study, the 808 nm pump light was shaped into a double-ring structure by the CDG and matched spatially with that of an ideal LG₁₁ mode. As a result, the laser resonator generated an LG₁₁ vortex mode, and the laser power reached 204 mW with 14.5% slope efficiency. Also, when the cavity mirror was tilted, the laser output could switch to the LG₀₁ vortex mode. The results showed the convenience and versatility of CDG in an annular-pumped vortex laser.

OCIS codes: 140.3580, 140.3480, 050.1950.
doi: 10.3788/COL201917.051402.

Laguerre–Gaussian (LG) modes, which are one set of eigen solutions of the Helmholtz equation under paraxial approximation in the cylindrical coordinate, exhibit doughnut-like transversal intensity distribution and possess a helical phase wave-front[1]. Generally, LG modes are described by $LG_{p,l}$, where p and l are the radial and azimuthal indices[2]. $LG_{p,l}$ modes with $l \neq 0$ have $p+1$ rings in the transverse field, and a helical phase front with topological charge of l carries a z component of orbital angular momentum (OAM) of $l\,\hbar$ per photon[3]. That is why LG modes are also called optical vortex beams[4]. Based on those physical properties, LG beams have been widely used in optical manipulation[5], optical communication in free space[6], super resolution microscopy[7], optical switching[8], and spinning object detection[9,10]. Compared with lower-order LG modes, high-order modes show superior performance in some fields[11,12]. For example, the high-order LG_{33} mode reduces the thermal noise of the mirrors, and its presence in the application of gravitational-wave detection signifies high sensitivity and a high detection rate[13–15].

The methods for generating LG modes include passive and active ways. The former refers to the spatial conversion of an incoming light beam after transmitting through the optical elements, like computed holograms[16], spiral phase plate[17], and spatial light modulator[18]. The latter aims to the direct oscillation of the desired LG mode in a laser resonator, either by deploying various mode selectors inside it[19] or applying the annular pumping technique[20–23]. As the annular pumping profile, after some shaping optics, intrinsically has good spatial overlapping with target LG modes in the gain medium, this technique favors the LG-mode excitation of one laser resonator with high efficiency and high modal purity.

As is known, a circular Dammann grating (CDG), a binary-phase component with periodic and alternate 0 and π phases in the radial direction, can diffract an incoming light into a single ring or multiple concentric rings with equal intensities at the far field[24,25]. We previously reported the utilization of a first-order CDG to implement a single-ring-pumped LG₀₁-mode neodymium-doped yttrium aluminum garnet (Nd:YAG) laser. This scheme is easy to realize by only inserting the CDG element into the laser's pump unit, and also, the fabrication of these elements is simple and with low cost.

In this study, to test the CDG's ability in assisting the excitation of high-order vortex mode, we firstly applied a second-order CDG to shape the pump light into a double-ring intensity profile at the far field; thereafter, we demonstrated the LG₁₁ mode's oscillation of a Nd:YAG laser. Furthermore, the LG₁₁ mode's oscillation was switched to the LG₀₁ mode stably when we slightly adjusted the inclination of the output coupler (OC) of the laser. The results showed the versatility of CDG-based annular pumping for a high-order LG-mode vortex solid-state laser.

Figure 1 shows the schematic diagram of the laser. An 808 nm fiber-coupled laser diode was used as the pump source, and its tail fiber had a core diameter of 105 μm and numerical aperture of 0.22. Behind the pigtail fiber, two lenses L_1 and L_2, with the focal lengths of 15 and 25.4 mm, respectively, were used to collimate the pump radiation and then focus it into the gain medium. The gain medium was a piece of Nd:YAG crystal that had 1 at. % doping concentration of Nd ions, 10 mm diameter, and 1 mm thickness. The front surface of it was coated for high transmission at 808 nm and high reflection at 1064 nm, and its rear surface was anti-reflection coated at 1064 nm.
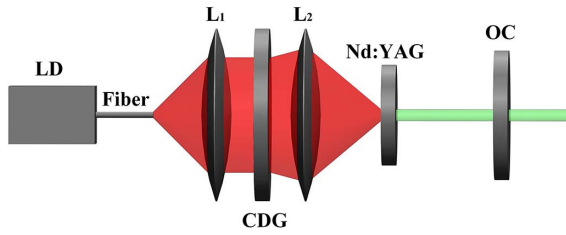
Fig. 1. Schematic diagram of an end-pumped laser involving a CDG in the pumping unit.

Both surfaces of the crystal clung to two large copper plates for cooling. In the central part of each copper plate, there was a 5 mm diameter hole drilled for light propagation. Further, a plane mirror with a transmittance of 2% at 1064 nm was placed behind the Nd:YAG crystal as an OC, and the distance between it and front surface of the crystal was 10 mm.

Except for the above-mentioned arrangement, a second-order CDG was placed between lenses L_1 and L_2. This CDG had a 25 mm clear aperture and was wet-etched on a substrate of BK7 glass in the form of concentric grooves with a 53.87 µm radial period and 790 nm depth. Figure 2(a) shows the surface view of the applied CDG taken by microscopy, in which the concentric and periodic structures were used to partition the profile of an incident pump beam and induce the periodic 0 and π phase shifts along the radial direction. Figure 2(c) plots the detailed structure of the CDG's cross section schematically along radial direction. As seen, three sets of combinations of the
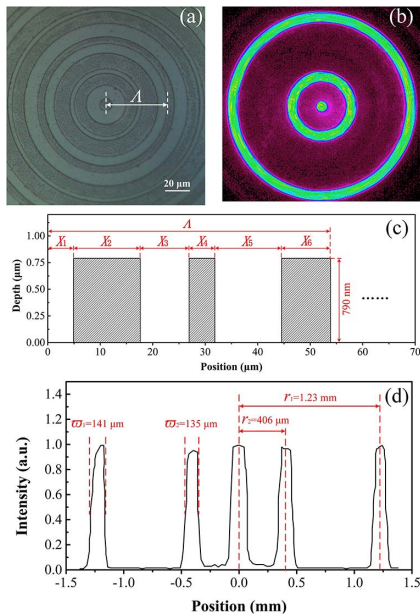

Fig. 2. (a) Top view of second-order CDG taken by microscopy, where the bright rings indicate the ridges, and the dark ones represent the grooves, (b) transverse intensity distribution of diffracted pump light at the far field, (c) schematic cross section of the CDG along the radial direction, and (d) the line profile of pump light along the radial direction.

ridges and grooves existed alternately in each period, and the theoretical widths of them were variable with the values of $X_1 = 4.91$ µm, $X_2 = 12.71$ µm, $X_3 = 9.31$ µm, $X_4 = 4.91$ µm, $X_5 = 12.71$ µm, and $X_6 = 9.31$ µm, respectively. With these parameters, this CDG would diffract only the first- and third-order pump light beams at 15 and 45 mrad diffraction angles with a theoretical diffraction efficiency of 80%.

The captured intensity distribution, as well as the corresponding line profile, of the pump light at the focus of L_2 is shown in Figs. 2(b) and 2(d). As observed, except for zero-order transmission, both the first- and third-order diffraction rings appeared at the far field with 406 µm and 1.23 mm ring radius, as well as 135 and 141 µm full width at half-maximum (FWHM), respectively. Therefore, the radius ratio of the outer and inner diffraction rings of pump light covered the range between $(r_1 + \varpi_1/2)/(r_2 - \varpi_2/2)$ and $(r_1 - \varpi_1/2)/(r_2 + \varpi_2/2)$, i.e., 3.84 and 2.45. Further, the radius ratio of the outer and inner rings of an ideal LG_{11} mode is nearly 3.21, which fell exactly in the range of the radius ratio of the pump diffraction rings, and thus, it had a good spatial match with the pump light field inside the resonator.

After the diffracted pump light was projected to the Nd:YAG laser crystal, the resonator cavity consisting of an OC and front surface of a laser crystal was optimized and began to oscillate at the pump level above the threshold. As shown in Fig. 3, when the absorbed pump power (P_{abs}) was larger than 1.02 W, the output power of the laser increased linearly with a slope efficiency of 14.5% and reached 204 mW at $P_{\mathrm{abs}} = 2.41$ W.

The intensity distribution of laser beams varied with pump power. Figure 4 depicted the captured intensity profiles of the laser beam at different pump powers.

As shown in Fig. 4(a), at $P_{\mathrm{abs}} = 1.06$ W, where the pump power was a little higher than the threshold, the laser produced a fundamental transverse electromagnetic (TEM_{00})-like mode. When the pump power increased and was smaller than 1.45 W, the laser showed the tendency to oscillate in the single-ring mode, as shown in Fig. 4(b). When P_{abs} was larger than 1.45 W, the double-ring structure of the laser mode appeared, with an obvious central null intensity, and such a shape was well-maintained in the range of 1.45 W $< P_{\mathrm{abs}} <$ 2.11 W. Further, when the pump power exceeded the level of
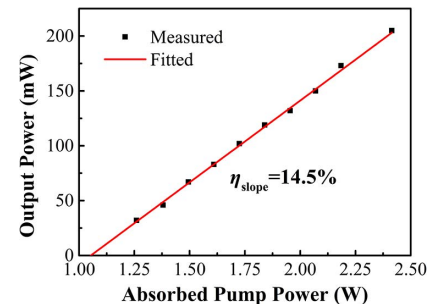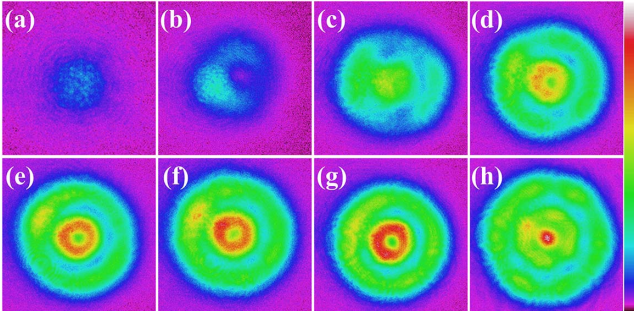

Fig. 3. Variation of output power of the laser with pump power.

Fig. 4. Intensity distributions of double-ring modes obtained at different pump powers: (a) $P_{abs} = 1.06$ W, (b) $P_{abs} = 1.17$ W, (c) $P_{abs} = 1.51$ W, (d) $P_{abs} = 1.65$ W, (e) $P_{abs} = 1.71$ W, (f) $P_{abs} = 1.83$ W, (g) $P_{abs} = 1.95$ W, and (h) $P_{abs} = 2.21$ W.

$P_{abs} = 2.21$ W, the double-ring structure of the laser beam remained, and additionally, the central null intensity of it was lightened. The difference between the output mode in Fig. 4(h) and the others could be attributed to the excitation of the TEM_{00} mode induced by the zero-order diffraction.

Then, the laser mode that had the double-ring intensity profile was analyzed. Figure 5 plots a one-dimensional intensity distribution of the laser mode obtained at $P_{abs} = 1.95$ W. Simultaneously, this measured line intensity profile was also fitted by using a linear superposition of a Laguerre-polynomial-modulated Gaussian function with the order of $2p + l$ (where $p = 1$ and $l = 1$) and a Gaussian function. As seen, the experimental curve agreed well with the theoretical profile of linear superposition of LG_{11} and TEM_{00} modes. Correspondingly, the output power shown in Fig. 3 included both LG_{11} and TEM_{00} modes, which meant that the actual output power of the LG_{11} mode was lower than experimental results. This comparison suggested that the intensity distribution of the obtained double-ring mode of the laser was principally made up of an ideal LG_{11} mode. Moreover, the existence of the TEM_{00} mode was associated with the excitation

induced by zero-order diffraction of second-order CDG, which was caused by the error of etching depth during fabrication. Therefore, the fraction of the TEM_{00} mode could be reduced by diminishing the error of absolute depth and improving the uniformity of etching depth in the grating plane to eliminate the zero-order diffraction of CDG. It means that it is possible to generate the pure LG_{11} mode with the well-fabricated second-order CDG.

Furthermore, the propagation behavior of the obtained double-ring mode was evaluated. Figure 6 depicts the variation of its waist diameter with propagation distance after the laser beam passed through a focusing lens. According to these curves, the quality factors M square (M^2) were calculated to be 4.42 in the x direction and 4.41 in the y direction, and these data were close to 4 for an ideal LG_{11} mode.

Finally, the interferometric technique was used to detect the phase of the obtained double-ring laser mode. Figure 7 shows the schematic setup of a Mach–Zehnder (M-Z) interferometer. The laser beam from the resonator was divided into two beams by a non-polarized beam splitter (NPBS). The beam in the upper arm was clipped by a 150 μm diameter pinhole, and then, the clipped fraction of the laser beam was collimated and acted as the plane reference wave. The laser beam in the lower arm was attenuated and acted as the signal wave. Both the reference beam and signal beam were directed into a charge-coupled device (CCD) camera, and Fig. 8 plots the measured interference pattern of them at $P_{abs} = 1.95$ W.

Theoretically, when the plane vortex beam and plane wave interferes, the Y-shaped fork would be formed near

Fig. 6. Evolution of beam waist of the laser mode at $P_{abs} = 1.95$ W along propagation distance. M^2, quality factors M square.
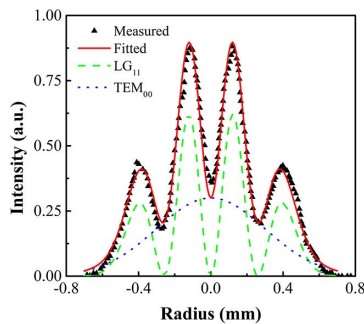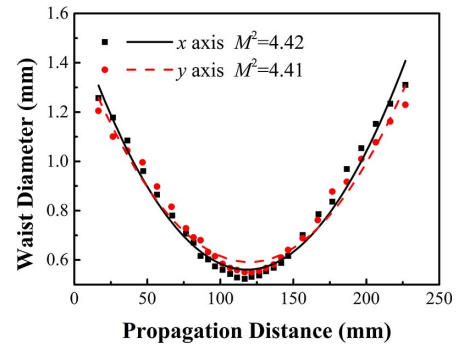

Fig. 5. Measured and theoretical intensity distribution of the laser mode along the horizontal direction at $P_{abs} = 1.95$ W. The black triangles represent the measured data points of the double-ring mode, the red line represents the theoretical profile of linear superposition of the LG_{11} and TEM_{00} modes, and the green and blue dashed lines represent the respective intensity profiles of theoretical LG_{11} and TEM_{00} modes.
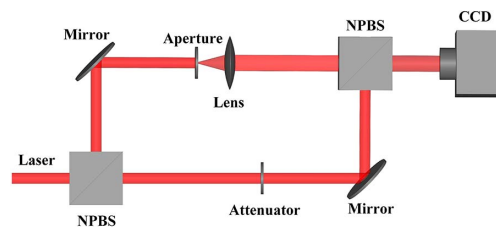

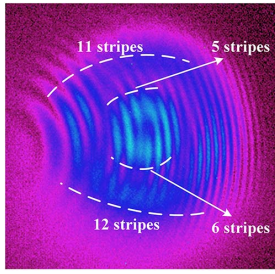Fig. 7. Schematic diagram of the Mach–Zehnder interferometer for phase detection. NPBS, non-polarized beam splitter.

Fig. 8. Captured interference patterns of the double-ring mode at $P_{abs} = 1.95$ W.

the phase singularity, and the numbers of the fork stand for the numbers of topological charge embodied in the helical phase. According to the interference pattern depicted in Fig. 8, the number difference between the upper and lower sides of the outer interference stripes, as well as the number difference between the upper and lower sides of the inner interference stripes, was one. Therefore, it could be inferred that both inner and outer rings of the double-ring laser mode had helical phases with respective topological charges of one, i.e., the double-ring laser mode from the resonator was the LG_{11} mode when P_{abs} was in the range of 1.45 to 2.11 W.

In our experiment, it was found that the double-ring laser mode could be switched to a single-ring mode when tilting the OC to a specific angle. Furthermore, single-ring-mode operation of the laser was stable, and the switching between double- and single-ring modes was producible. Figure 9 depicts the variation of output power with pump power when the laser was operated in the single-ring mode. As seen, at this time, this laser had the threshold pump power of $P_{abs} = 1.36$ W, and the output power increased linearly with P_{abs} at a slope efficiency of 14.7% and reached its maximum of 77 mW

at $P_{abs} = 1.91$ W. The intensity distributions of the laser mode at different pump power were shown in Fig. 10. As seen, the laser beam was at the TEM_{00} mode at low pump power close to the threshold and transformed into the single-ring mode at $P_{abs} = 1.47$ W. Further, the single-ring intensity distribution of the laser mode maintained until P_{abs} reached 1.71 W. When P_{abs} exceeded 1.71 W, the axis symmetry of the single-ring mode started to deteriorate, and its shape tended to be irregular.

Then, the measured intensity distribution of the single-ring mode along the horizontal direction at $P_{abs} = 1.64$ W was fitted by a Laguerre-polynomial-modulated Gaussian function with the order of $2p + l$ (where $p = 0$ and $l = 1$). As shown in Fig. 11, the measured curve had a great agreement with their respective theoretical data, and this comparison suggested the intensity distribution of the obtained single-ring mode of the laser was identical to that of an ideal LG_{01} mode. Also, the evolution of beam waist diameter along propagation distance was measured at $P_{abs} = 1.64$ W and shown in Fig. 12. The beam quality factor M^2 was measured to be 2.41 in the x direction and 2.10 in the y direction, and these data were close to 2 for an ideal LG_{01} mode. Furthermore, the M-Z interferometer was used to detect the phase structure of the obtained single-ring mode, and the interference patterns are shown in Fig. 13. The Y-shaped structure in the central region indicated that the single-ring mode from the Nd:YAG laser resonator had a helical phase with a topological charge of one, i.e., the single-ring laser mode from the resonator was the LG_{01} mode when P_{abs} was in the range of 1.41 to 1.71 W.

Fig. 11. Measured and theoretical intensity distribution of the laser mode along the horizontal direction at $P_{abs} = 1.64$ W.
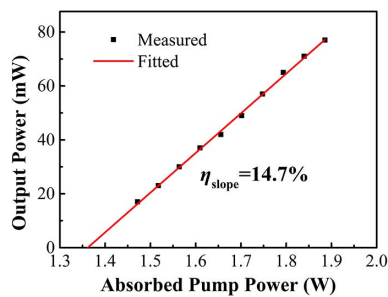

Fig. 9. Variation of output power of the laser with pump power.

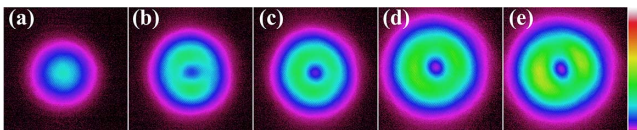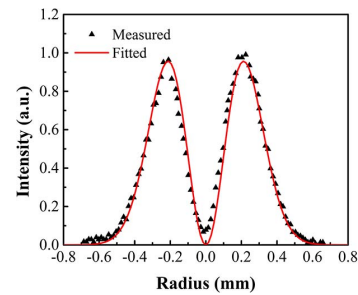

Fig. 10. Intensity distributions of single-ring modes obtained at different pump powers: (a) $P_{abs} = 1.37$ W, (b) $P_{abs} = 1.47$ W, (c) $P_{abs} = 1.51$ W, (d) $P_{abs} = 1.64$ W, and (e) $P_{abs} = 1.71$ W.
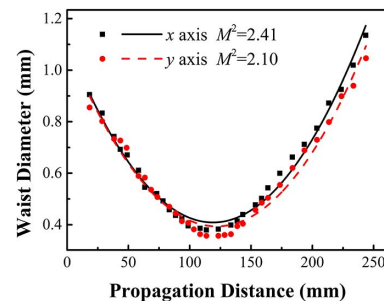

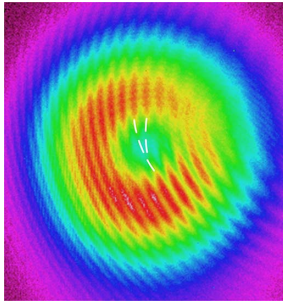Fig. 12. Evolution of the beam waist of the laser mode at $P_{abs} = 1.64$ W along the propagation distance.

Fig. 13. Captured interference patterns of the single-ring mode at $P_{abs} = 1.64$ W.

In the experiment, with an optimized parallel cavity structure, the resonator generated the double-ring LG_{11} mode, while with tilted OC, the laser emitted the single-ring LG_{01} mode. Such a mode switching phenomenon was associated with the variation of intracavity mode loss.

As known, both LG_{11} and LG_{01} modes are eigen modes of the circular mirror cavity. In the resonator with a parallel cavity, the intracavity losses of both modes were at a relatively low level. In the optimized parallel cavity, the LG_{11} mode had the highest spatial overlapping efficiency with pump light field, and it could extract most of stored gain and thus dominated in the mode competition. As a result, the parallel cavity laser resonator emitted the LG_{11} mode when P_{abs} was in the range of 1.45 to 2.11 W. Compared with the low-order LG_{01} mode, the LG_{11} mode had a much larger divergence angle, and therefore, the diffraction loss of it increased rapidly with the tilt angle of the OC. Although the LG_{01} mode had relatively lower spatial overlapping efficiency with the double-ring pump light field, it became dominated in mode competition because of its low diffraction loss when the OC was tilted. As a result, the laser emission switched to the LG_{01} mode when P_{abs} was in the range between 1.41 and 1.71 W, and the corresponding power of the LG_{01} mode was lower than the case of LG_{11}-mode operation, owing to the increase of the total intracavity loss.

Although the LG_{01} mode was obtained in lasers with first- and second-order CDG by annual pumping, we think there are some differences in principle. The LG_{01} mode was generated from the laser with first-order CDG for its high spatial overlapping efficiency, while it was generated from the laser with second-order CDG and tilted OC for its low diffraction loss.

In summary, we proposed an LG_{11}-mode Nd:YAG laser by applying a second-order CDG to shape the pump light into a double-ring pump field, and the LG_{11}-mode power of the laser reached 204 mW with a slope efficiency of 14.5%. The further experiment showed that the LG_{11}-mode laser could be switched to the LG_{01} mode stably by slightly adjusting the tilt angle of the OC.

The results showed the versatility of high-order CDG for an annular pumping high-order vortex-mode solid-state laser. The performance of our laser still had a large space to promote. Specifically, the diffraction efficiency of the used grating could be increased by applying anti-reflection coating, where the zero-order transmission of it could be eliminated by optimizing the fabrication, and the quality of the vortex laser mode at high pump power could be improved further by optimizing the cooling to the laser crystal.

References

1. L. Allen, M. J. Padgett, and M. Babiker, Prog. Opt. **39**, 291 (1999).
2. X. Liu, T. Wu, L. Liu, C. Zhao, and Y. Cai, Chin. Opt. Lett. **15**, 030002 (2017).
3. L. Allen, M. W. Beijersbergen, R. J. C. Spreeuw, and J. P. Woerdman, Phys. Rev. A **45**, 8185 (1992).
4. J. E. Curtis and D. G. Grier, Phys. Rev. Lett. **90**, 133901 (2003).
5. D. G. Grier, Nature **424**, 810 (2003).
6. J. Wang, Photon. Res. **4**, B14 (2016).
7. P. Torok and P. R. T. Munro, Opt. Express **12**, 3605 (2004).
8. A. E. Willner, L. Li, G. Xie, Y. Ren, H. Huang, Y. Yue, N. Ahmed, M. J. Willner, A. J. Willner, Y. Yan, Z. Zhao, Z. Wang, C. Liu, M. Tur, and S. Ashrafi, Photon. Res. **4**, B5 (2016).
9. M. P. J. Lavery, F. C. Speirits, S. M. Barnett, and M. J. Padgett, Science **341**, 537 (2013).
10. G. Milione, T. Wang, J. Han, and L. Bai, Chin. Opt. Lett. **15**, 030012 (2017).
11. M. A. Clifford, J. Arlt, J. Courtial, and K. Dholakia, Opt. Commun. **156**, 300 (1998).
12. N. B. Simpson, L. Allen, and M. J. Padgett, J. Mod. Opt. **43**, 2485 (1996).
13. M. Granata, C. Buy, R. Ward, and M. Barsuglia, Phys. Rev. Lett. **105**, 231102 (2010).
14. P. Fulda, K. Kokeyama, S. Chelkowski, and A. Freise, Phys. Rev. D **82**, 012002 (2010).
15. S. Chelkowski, S. Hild, and A. Freise, Phys. Rev. D **79**, 122002 (2009).
16. N. R. Heckenberg, R. McDuff, C. P. Smith, and A. G. White, Opt. Lett. **17**, 221 (1992).
17. M. W. Beijersbergen, R. P. C. Coerwinkel, M. Kristensen, and J. P. Woerdman, Opt. Commun. **112**, 321 (1994).
18. N. Matsumoto, T. Ando, T. Inoue, Y. Ohtake, N. Fukuchi, and T. Hara, J. Opt. Soc. Am. A **25**, 1642 (2008).
19. S. Tan, C. Zhou, A. Shirakakwa, K. Ueda, and J. Li, Opt. Laser Technol. **96**, 76 (2017).
20. Z. Fang, K. Xia, Y. Yao, and J. Li, Appl. Phys. B **117**, 219 (2014).
21. J. Li, Y. Yao, J. Yu, K. Xia, and C. Zhou, IEEE Photon. Technol. Lett. **28**, 473 (2016).
22. Y. Xu, X. Han, G. Li, J. Liu, K. Xia, and J. Li, Opt. Eng. **55**, 056101 (2016).
23. Y. Wu, Z. Wang, S. Chen, A. Shirakwa, K. Ueda, and J. Li, Laser Phys. Lett. **15**, 055804 (2018).
24. C. Zhou and L. Liu, Appl. Opt. **34**, 5961 (1995).
25. C. Zhou, J. Jia, and L. Liu, Opt. Lett. **28**, 2174 (2003).